# Reaction Force Analysis of the Effect of Mg(II) on the 1,3 Intramolecular Hydrogen Transfer in Thymine

**Elizabeth Rincón, Pablo Jaque, and Alejandro Toro-Labbé***

*QTC, Departamento de Química Física, Facultad de Química, Pontificia Universidad Católica de Chile, Casilla 306, Correo 22, Santiago, Chile*

*Received: May 10, 2006; In Final Form: May 25, 2006*

The 1,3 intramolecular hydrogen transfer reaction in free thymine and in Mg(II)−thymine have been studied at the density functional theory level. The mechanism of intramolecular proton transfer in these systems emerges from the analysis of the reaction force profile along the reaction path; it is rationalized in terms of structural and electronic reorganizations that take place during the chemical transformation. Results show that the presence of Mg(II) monocoordinated to thymine activates the hydrogenic motion by inducing structural and electronic changes in the molecular backbone. In the metallic complex, it is found that the hydrogen transfer is followed by a relaxation process that facilitates the metal cation migration to form a bicoordinated complex.

## 1. Introduction

In this work, we present a theoretical study of the effect of Mg(II) in the keto ⇌ enol tautomerization reaction in thymine (Figure 1). The intramolecular proton transfer occurring in thymine and in Mg(II)−thymine is characterized through the analysis of the energy and reaction force profiles (Figure 2); the information about the mechanism of the transfer is obtained through the simultaneous analysis of the evolution along the reaction coordinate of few key structural and electronic properties. This information together with the characterization of transition states allows one to identify the properties that are activated or inhibited along the reaction coordinate, thus defining the processes that are driving the reaction.

The reaction force is the negative of the derivative of the potential energy with respect to the reaction coordinate ($\omega$); its profile identifies three regions along $\omega$:[1−8] the reactant region in which a preparation step activates the reaction in most cases through structural reordering to reach a reactive complex; the transition state region, which is often characterized by a marked electronic reordering; and the product region, where the structural relaxation leads to products. To each of these regions a specific amounts of work can be associated to quantify the energetic cost of each process.[1−8]

In this paper, we have focused on the application of the above-mentioned concepts to gain insight on the effect of the metal cations on the stability and reactivity at biomolecules.[9−13]

The excess of several cations have been related with highly toxic effects, including tumor development,[14] whereas the decrease of physiologically accepted levels of metal cations has been related with the appearance of diseases, such as, for instance, *hypomagnesaemia*, which is the magnesium deficiency observed in patients under anticancer treatments.[15] In this context, the characterization of the interactions between metal cations and biomolecules is of high interest in biochemistry and coordination chemistry. In the last three decades, both experimental and theoretical studies have been performed to improve the understanding of these interactions and, particularly, how the metal cations regulates many processes within the living organisms.

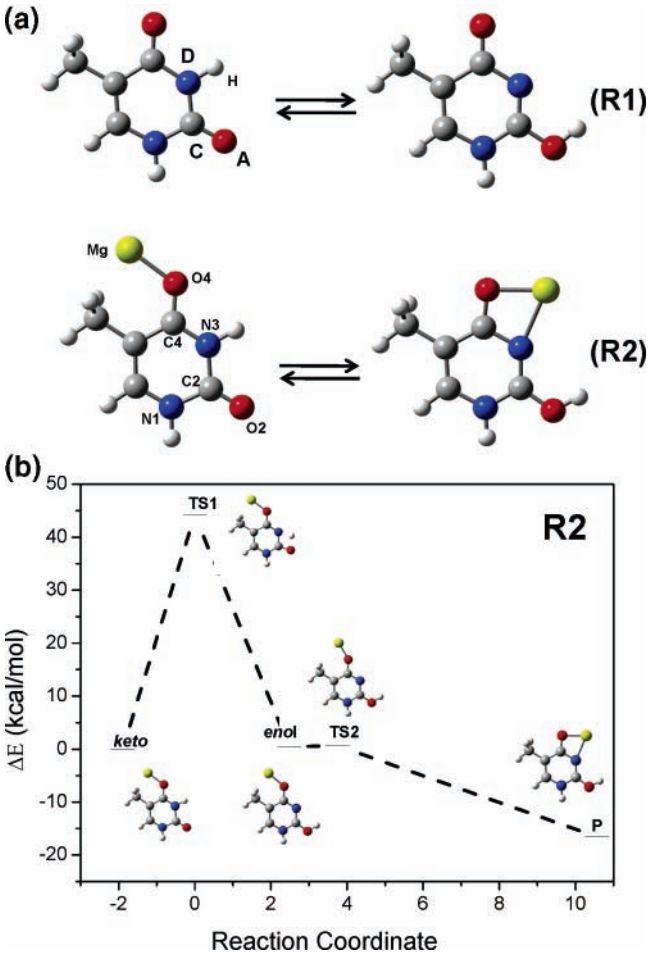


**Figure 1.** (a) Sketch of the hydrogen transfer processes in free thymine (**R1**) and Mg(II)−thymine complex (**R2**). (b) Relative energy diagram for the two-step sequential process in Mg(II)−thymine complex.

* To whom correspondence should be addressed. E-mail: atola@puc.cl.

10.1021/jp062870u CCC: $33.50 
Published on Web 07/11/2006

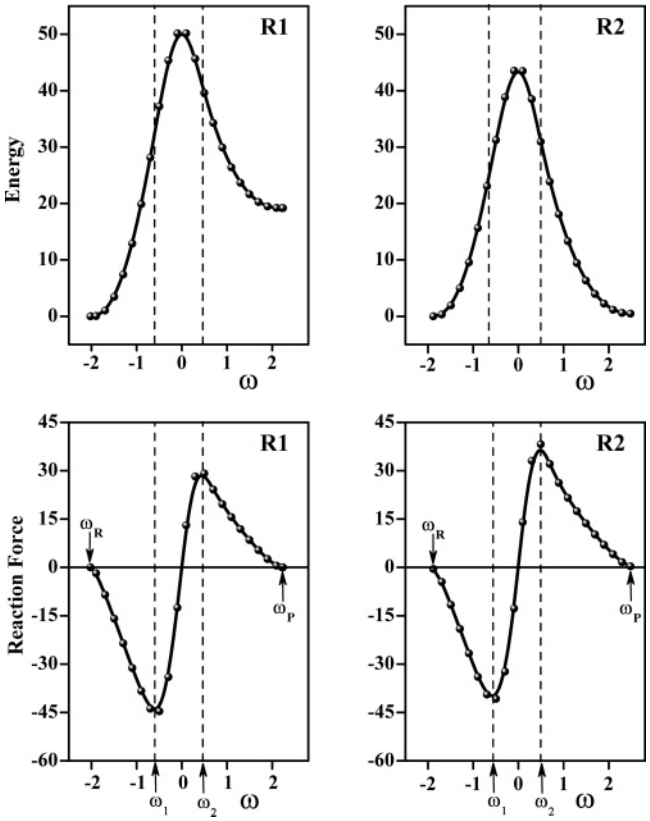


**Figure 2.** Relative energy (in kcal/mol) and force profiles (in kcal/mol·w) of the 1,3 intramolecular hydrogen transfer in **R1** and **R2**. The dashed vertical lines indicates the limits of the different regions identified from the force profiles.

Magnesium is a divalent cation characterized by a small ionic radius (0.86 Å); these properties, charge and size, are responsible for its formation of many stable complexes with ligands of different natures. Mg(II), the second most important intracellular cation after potassium, plays a significative role in the stabilization of the secondary and tertiary structures of DNA.[15,16] This macromolecule presents a large amount of essential biochemical processes that could be affected by the presence of Mg(II).[17,18] Studies on isolated nucleotides have shown that magnesium ions form stable complexes with the DNA bases themselves.[19−22] One of the effects of the presence of metal cations bound to the DNA bases is that it may induce tautomeric transformation in nucleobases:[23,24] the keto and amino tautomers, which are the dominant species in the DNA double helix, are converted into their counterparts enol and imino forms, respectively.[25] At the biochemical level, the tautomeric interconvertion in DNA is considered as a possible molecular mechanism that may produce spontaneous mutations and activation of cancer processes.[26−28] In the last years, several studies[13,22] have been focused to characterize the interaction Mg(II)−DNA; although these investigations have contributed to improve our understanding on the nature of the interaction, the effect of Mg(II) on the tautomerization processes that may take place in the nucleobases has not yet been reported; this is the matter of this work.

The goal of this study is 2-fold: first, characterization of the mechanism that controls the intramolecular hydrogen transfer reaction in thymine and Mg(II)−thymine (Figure 1a); second, analysis of the migration process that take over after the hydrogen transfer process and brings the Mg(II)−thymine (keto) monocoordinated complex into Mg(II)−thymine (enol) bicoordinated complex (Figure 1b). This paper is organized as follows: in Section 2, we present the theoretical elements for the analysis of the reactions; Section 3 describes the computational methods employed; Section 4 presents the results and discussion; and in Section 5, the main conclusions are drawn.

## 2. Theoretical Background

**The Reaction Force**. The energy profile along a reaction coordinate, $E(\omega)$, describes the energetic change when reactants (**R**) are getting transformed into products (**P**) passing by a transition state (**TS**), the highest point of the energy profile. $E(\omega)$ provides the thermodynamic and kinetic information of a chemical reaction, but it does not gives insights on the reaction mechanism. The concept of a reaction mechanism is closely related with the nuclear displacements that occur when going from reactants to products.[1−8] These displacements are related with the net force acting on the system as the reaction takes place along the reaction coordinate; accordingly, the reaction force is defined as the derivative of the potential energy $E(\omega)$:[1]

$$F(\omega) = -\frac{\mathrm{d}E}{\mathrm{d}\omega} \tag{1}$$

For a chemical reaction in which reactants and products are separated by an energy barrier, $F(\omega)$ presents two critical points: a minimum located at $\omega_1$ before reaching the transition state and a maximum located at $\omega_2$ after the **TS**. These critical points define regions along the reaction coordinate where different mechanisms might be operating through the activation or inhibition of specific interactions that might be of different nature.[1−8] The reactant region is defined within the interval $\omega_R \leq \omega \leq \omega_1$; this is the region where the reactants are prepared to chemical transformation, mainly through structural reordering that leads to a reactive complex at $\omega_1$. The **TS** region is defined within the interval between the minimum and maximum of the force profile ($\omega_1 < \omega < \omega_2$); this region is mainly characterized by electronic reordering. The interval $\omega_2 \leq \omega \leq \omega_P$ defines the product region where the molecular structures relax until reaching the product equilibrium geometry.

The work associated to the process occurring at the reactants region is given by:

$$W_1 = -\int_{\omega_R}^{\omega_1} F(\omega)\mathrm{d}\omega \tag{2}$$

and the work necessary to reach the transition state from the reactive complex at $\omega_1$ is:

$$W_2 = -\int_{\omega_1}^{\omega_{TS}} F(\omega)\mathrm{d}\omega \tag{3}$$

Thus, the activation energy for the forward reaction is written in terms of two contributions that are expected to be of different nature:

$$\Delta E^{\ddagger}_{for} = W_1 + W_2 \tag{4}$$

For the forthcoming analysis, we also define:

$$W_3 = -\int_{\omega_{TS}}^{\omega_2} F(\omega)\mathrm{d}\omega;\ W_4 = -\int_{\omega_2}^{\omega_P} F(\omega)\mathrm{d}\omega \tag{5}$$

such that $\Delta E^{\ddagger}_{rev} = \Delta E^{\ddagger}_{for} - \Delta E^{\circ} = -W_3 - W_4$, with the reaction energy $\Delta E^{\circ} = W_1 + W_2 + W_3 + W_4$ and $\Delta E^{\ddagger}_{rev}$ being the activation energy for the reverse reaction.

**Characterization of Transition States**. The energy barrier [$\Delta E^{\ddagger}_{for} = E(\mathrm{TS}) - E(\mathrm{R})$] can be rationalized through the Marcus equation (ME), which is defined as:.[8,29,30]

$$\Delta E_{for}^{\ddagger} = \Delta E_0^{\ddagger} + \frac{1}{2}\Delta E^{\circ} + \frac{(\Delta E^{\circ})^2}{16\Delta E_0^{\ddagger}} \quad (6)$$

where $\Delta E^{\circ} = E(P) - E(R)$ is the reaction energy and $\Delta E_0^{\ddagger}$ is the so-called Marcus' intrinsic activation energy. It has been shown that $\Delta E_0^{\ddagger}$ is related to the force constants associated to the reactive mode of reactants ($k_R$) and products ($k_P$) through the following equation:[8]

$$\Delta E_0^{\ddagger} = \frac{1}{4}(k_R + k_P) \quad (7)$$

thus indicating that the intrinsic barrier is basically a structural quantity.[29] In summary, the Marcus Equation links the energy barrier with the reaction energy through the intrinsic barrier.

On the other hand, the ME is consistent with the Bell−Evans−Polanyi (BEP) principle and the Hammond postulate (HP).[31,32] The first states that for similar reactions the more exothermic (endothermic) reaction will have the lower (higher) activation energy, whereas the HP relates the position of the **TS** to the exothermicity of the reaction. The HP is quantified through the Brønsted coefficient, $\beta$, which is defined as:[33]

$$\beta = \frac{\partial \Delta E_{for}^{\ddagger}}{\partial \Delta E^{\circ}} = \frac{1}{2} + \frac{\Delta E^{\circ}}{8\Delta E_0^{\ddagger}} \quad (8)$$

Following the Leffler postulate, $\beta$ is a measure of the similarity of the **TS** with respect to the product of the reaction.[32,34] It can also be interpreted as the position of the **TS** in a reduced reaction coordinate that goes from 0 (reactants) to 1 (products).[30] These definitions predicts that an exoenergetic reaction will present a reactant-like (or earlier) transition state ($\beta < (1/2)$), whereas a product-like (or later) transition state ($\beta > (1/2)$) will characterize endoenergetic processes. In symmetric reactions ($\Delta E^{\circ} = 0$), the transition state is found at midway between reactant and product, thus $\beta = (1/2)$. The above analysis shows the consistency between the Marcus equation[29] with the Bell−Evans−Polanyi principle and the Hammond postulate.[31,32]

**Chemical Potential and Hardness.** Chemical potential ($\mu$) and hardness ($\eta$) are global electronic properties that describe the reactivity of molecular systems and have been defined within the so-called conceptual density functional theory (DFT) as follows:[35,36]

$$\mu = \left(\frac{\partial E}{\partial N}\right)_{v(\vec{r})} \quad \eta = \frac{1}{2}\left(\frac{\partial^2 E}{\partial N^2}\right)_{v(\vec{r})} \quad (9)$$

The electronic chemical potential ($\mu$) measures the escaping tendency of the electronic cloud from equilibrium,[37] and molecular hardness can be seen as a resistance to charge transfer.[38] Using a finite difference approximation and the Koopmans' theorem, these quantities can be estimated through the following operational formulas:[35,39]

$$\mu \approx \frac{1}{2}(\epsilon_L + \epsilon_H) \quad \eta \approx \frac{1}{2}(\epsilon_L - \epsilon_H) \quad (10)$$

where $\epsilon_H$ and $\epsilon_L$ are the energies of the highest occupied and lowest unoccupied molecular orbitals, HOMO and LUMO, respectively.

## 3. Methods and Computational Details

All geometries involved in the reaction path were fully optimized at the B3LYP/6-311++G(d,p) level of theory.[40] The minima and saddle-point on the potential energy surfaces were also confirmed by frequency calculations at the MP2/6-311++G(d,p) level.[41] Transition states were determined through the quadratic synchronous transit (QST2) methodology.[42] The minimum energy path in going from reactants to products were calculated through the intrinsic reaction coordinate procedure ($\omega$ = IRC).[43] The profiles of energy, force, structural parameters, and electronic properties were obtained through single-point calculations on the previously optimized geometries given by the IRC procedure. Natural bond order (NBO)[44] population analysis was carried out to have a close view on the evolution of local electronic properties along the reaction coordinate. All calculation were performed with the GAUSSIAN 03 code.[45]

## 4. Results and Discussion

**4.1. Energetic Analysis.** Figure 1a sketches the systems under study: reaction 1 (**R1**) is the 1,3 intramolecular hydrogen transfer in free thymine; reaction 2 (**R2**) is a two step reaction: the first step is the 1,3 hydrogen transfer to produce the Mg−thymine(*enol*) monocoordinated complex, and the second step is the migration of the metal to produce a Mg−thymine(*enol*) bicoordinated complex, see Figure 1b.

The energy profiles for the 1,3 intramolecular hydrogen transfer in thymine and Mg−thymine are displayed in Figure 2 (upper panels); Table 1 contains the energetic information characterizing **R1** and the hydrogen transfer step of **R2**. Whereas **R1** is an endoenergetic reaction ($\Delta E^{\circ} = 19.10$ kcal/mol), in **R2**, the keto and enol isomers present about the same energy ($\Delta E^{\circ} = 0.45$ kcal/mol). However, the global energy change in **R2** after the two-step reaction is achieved is $\Delta E^{\circ} = -19.11$ kcal/mol, Figure 1b. Thus, the presence of Mg(II) stabilizes the *enol* tautomer of thymine; these results are in agreement with the experimental data reported by Liu et al,[19] which concluded that the proximity of a positive charge provided by a metal cation stabilizes the nucleobases.

The DFT energetic barrier of the hydrogenic motion along the keto → enol interconversion in **R2** is $\Delta E_{for}^{\ddagger} = 44.21$ kcal/mol (Table 1); in this first step, the metal cation remain attached to O4 (Figure 1) so that the enolic stable complex can be seen as an intermediate species that initiates the reaction that leads to the formation of a bicoordinated complex, with O4 and N3 being the chelation sites. The formation of Mg(II)−thymine (enol) indicates that the 1,3 intramolecular hydrogen-transfer process is necessary to activate the migration of the metal cation.

**Energy Barriers**. Using $\Delta E^{\circ}$ and $\Delta E_{for}^{\ddagger}$ as inputs for the Marcus equation (see eq 6), the intrinsic energy barrier $\Delta E_0^{\ddagger}$ can be estimated; the values are quoted in Table 1. The intrinsic barrier of **R1** is lower than that of **R2** due to the high thermodynamical contribution to $\Delta E_{for}^{\ddagger}$ in **R1**. As already mentioned, the presence of the metal cation favors the formation of the enol tautomer by 19 kcal/mol; however, the energy barriers $\Delta E_{for}^{\ddagger}$ and $\Delta E_0^{\ddagger}$ of **R1** and **R2** differ only by 5.4 and 4.5 kcal/mol, respectively; $\Delta E_{for}^{\ddagger}$ (**R1**) > $\Delta E_{for}^{\ddagger}$ (**R2**), thus indicating that the cation helps activation of the hydrogen transfer. However, the intrinsic barriers that are mainly due to structural effects behave differently, $\Delta E_0^{\ddagger}$ (**R1**) < $\Delta E_0^{\ddagger}$ (**R2**), thus suggesting that the cation is conferring some extra rigidity to the vibrational modes of the backbone structure, thus rising the structural barrier.

It can be noticed in Table 1 that the $\Delta E_{for}^{\ddagger}$'s values for the forward reactions (keto → enol) are higher than the $\Delta E_{rev}^{\ddagger}$'s values for the reverse reactions; this trend is especially marked in **R1**, again due to the high $\Delta E^{\circ}$ value. In the case of **R2**,

**TABLE 1: Reaction Energy ($\Delta E°$); Forward ($\Delta E^{\ddagger}_{for}$), Reverse ($\Delta E^{\ddagger}_{rev}$), and Intrinsic ($\Delta E^{\ddagger}_{0}$) Energy Barriers; Brönsted Coefficient $\beta$; and the Amount of Work Associated to the Different Processes in the 1,3 Intramolecular Hydrogen Transfer[a]**

| reaction | $\Delta E°$ | $\Delta E^{\ddagger}_{for}$ | $\Delta E^{\ddagger}_{rev}$ | $\Delta E^{\ddagger}_{0}$ | $\beta$ | $W_1$ | $W_2$ | $-W_3$ | $-W_4$ |
|---|---|---|---|---|---|---|---|---|---|
| **R1** | 19.10 | 49.61 | 30.51 | 39.48 | 0.56 | 32.64 | 16.97 | 7.00 | 23.51 |
| **R2** | 0.45 | 44.21 | 43.76 | 43.98 | 0.50 | 27.11 | 17.10 | 9.37 | 34.39 |

[a] All values in kcal/mol.

$\Delta E^{\ddagger}_{for} \approx \Delta E^{\ddagger}_{rev}$, thus indicating that the chemical characteristics of the donor−acceptor couples of the forward and reverse reactions are playing different roles than in **R1**. Nitrogen and oxygen atoms present quite similar proton affinities (118.1 and 116.1 kcal/mol, respectively);[46] in these terms, the energy barriers for the forward and reverse reaction are expected to be quite close to each other. However, in **R1**, the proton affinities of N3 seem to be strenghtened by the vicinity of the O4 atom (see Figure 1), thus producing considerably different values for the forward and reverse energy barriers. The presence of the Mg cation in **R2** bonded to O4 brings back the behavior expected on the basis of the nitrogen and oxygen proton affinities only: the energy barrier for the forward and reverse reactions are quite close to each other. In summary, $\Delta E°$, $\Delta E^{\ddagger}_{for}$, and $\Delta E^{\ddagger}_{0}$ values indicate that the presence of Mg(II) favor the keto → enol interconversion in thymine from the kinetic and thermodynamic viewpoints.

The Brönsted coefficients, also quoted in Table 1, indicate that the **TS** in **R1** is structurally and energetically closer to the product. In **R2**, the $\beta$ value indicates that the **TS** is practically at midway between the keto and enol forms. We shall see that the profiles of structural and electronic properties along the reaction coordinate confirm the similarity of the **TS** with respect to reactants or products suggested by the Brönsted coefficient.

**Reaction Force.** The reaction force profiles associated to both reactions are also displayed in Figure 2. The key points along the intrinsic reaction coordinate of **R1** and **R2** are the critical points on the force profiles or the inflection points on the energy profiles; the position of these points and the regions they define are indicated by vertical dashed lines that are also shown in the profiles of energy and forthcoming properties discussed in this study.

It has been shown[4−7] that processes occurring in the reactant region ($\omega_R \le \omega \le \omega_1$) are mostly related to displacements of the donor and acceptor atoms to get close enough to promote the hydrogen transfer. This is the preparation step of the reaction that leads to a reactive complex; the transition state region ($\omega_1 < \omega < \omega_2$) is mainly characterized by electronic reordering processes, and in the product region ($\omega_2 \le \omega \le \omega_P$), a structural relaxation brings the donor and acceptor atoms far away to reach the equilibrium geometry of the product. To each of the above-mentioned processes there is associated a specific amount of work that are defined in eqs 2, 3, and 5 and quoted in Table 1. Note that the $W_2$ values of **R1** and **R2** are quite close to each other; because the energy barrier can be expressed as $\Delta E^{\ddagger}_{for} = W_1 + W_2$, it can be concluded that it is the difference between the $W_1$ values, which explains the observed difference in the energetic barriers of **R1** and **R2**.

The amount of work in the product region, $W_4$, is higher in **R2** than **R1** by about 11 kcal /mol; this explains part of the stabilization conferred by the presence of Mg(II) to the enol tautomer, with this stabilization being responsible for the high-energy barrier of the reverse reaction in **R2**. The energies $W_2$ and $W_3$ are mainly associated to electronic rearrangements that promote the actual hydrogen transfer through the reordering of the electron density in the H−N3−C2−O2 skeleton. We observe that $W_2$ and $W_3$ are quite similar in both reactions; this indicates that the hydrogen transfer itself is basically not affected by the presence of the metal cation. These results show that the effect of the metal cation on $\Delta E^{\ddagger}_{for}$ is contained in $W_1$ rather than in $W_2$.

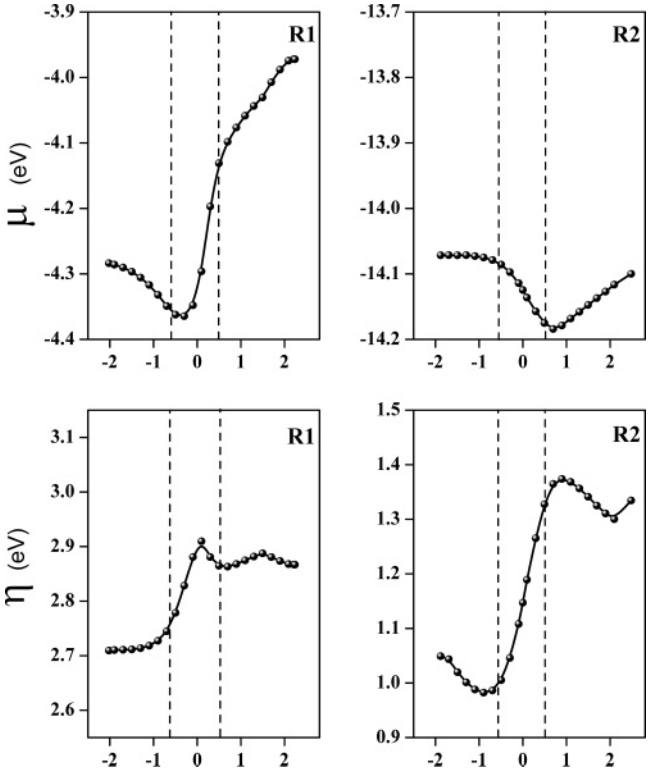


**Figure 3.** Chemical potential and hardness profiles (in eV) along $\omega$ for **R1** and **R2**.

**4.2. Chemical Potential and Hardness.** It can be noticed in Figure 3 that the most important changes exhibited by these electronic properties occur at the transition state region, thus confirming that this is the region where most electronic reordering is taking place.

In **R1**, $\mu$ decreases, reaching a minimum near $\omega_1$, and then it increases sharply at the **TS** and product regions. Contrary to this, in **R2**, $\mu$ remains quite constant until $\omega_1$, when then it decreases to reach a minimum at the vicinity of $\omega_2$, and then it increases until the product is formed. In contrast to **R1**, the chemical potential of the reactant and product of **R2** present quite similar values; this indicates that **R1** proceeds with larger electronic reordering than **R2**. From the hardness perspective, the lowering in the forward barrier in **R2** is due to the fact that the reactive complex at $\omega_1$ is softer than that of **R1**, and the chemical potential for this reaction remains constant at the vicinity of $\omega_1$. In the **R1** reverse reaction, $\eta$ presents a constant value at the vicinity of $\omega_2$, whereas for that in **R2**, the $\eta$ profile presents a maximum when approaching $\omega_2$ from the product; the order $\Delta E^{\ddagger}_{rev}(\mathbf{R2}) \gg \Delta E^{\ddagger}_{rev}(\mathbf{R1})$ should be, in part, associated to the larger variation of $\eta$ in the product region of **R2** with respect to the variation of $\eta$ within the same region in **R1**.

**4.3 Structural Properties**. Many metal−nucleobase complexes have been characterized by X-ray methods;[24,47] these

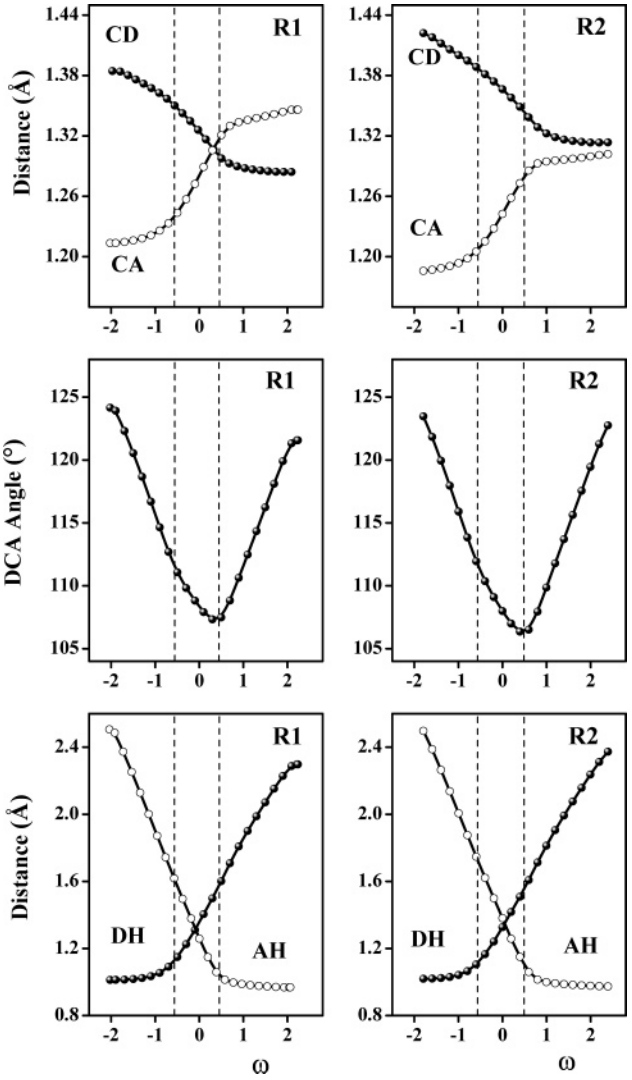


**Figure 4.** Bond distances and angles profiles (in Å and degrees, respectively) within the reactive backbone of **R1** and **R2**.

experiments show that when the metals' cations are alkaline or alkaline earth, they are bound to exocyclic oxygens, thus preventing dramatic changes in bond lengths, angles, and ring planarity.[48] However, there are some specific vibrational modes that contribute to explain the hydrogenic transfer mechanism in free thymine and in the Mg(II)−thymine complex. Figure 4 shows the evolution along $\omega$ of bond distances and angles associated to the atoms that are directly involved in the 1,3 intramolecular hydrogen transfer.

It can be noticed that the distance between the adjacent carbon and the donor atom, (**CD**), decreases quite monotonically until $\omega_2$ (maximum in the force profile); afterward, it remains practically constant. The **CA** (carbon-acceptor atom) bond distance remains nearly constant in the reactant region, and then it increases sharply in the **TS** region to reach the product region where, again, it remains reasonably constant. The trends observed in the **CD** and **CA** are indicating the gain and loss of double-bond character, respectively. In **R1**, this characteristic is marked by the **CD**−**CA** crossing near $\omega_2$; in **R2**, no such crossing is observed, although within the product region, **CD** and **CA** tend to a similar value, thus indicating that Mg(II) favors delocalization in the **D**−**C**−**A** backbone. These changes in bond distances along $\omega$ indicate that these are active modes in promoting the hydrogen transfer. On the other hand, in **R1** the **CD** and **CA** distances in the reactants region are closer to each other than in **R2**; the opposite situation is observed in the product region; this is possibly due to an increment of the electronic delocalization induced in the product region by the presence of the metal cation.

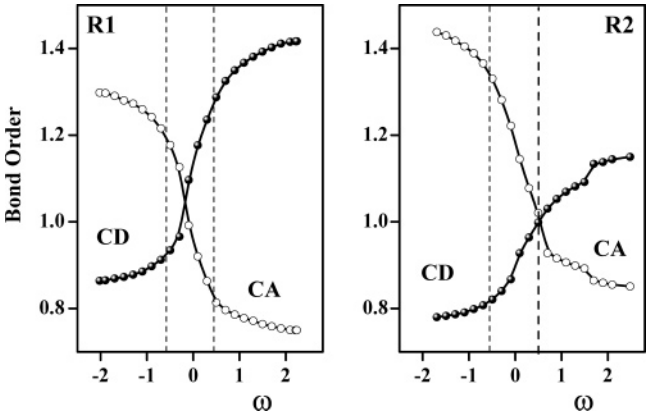


**Figure 5.** Bond orders profiles for **CA** and **CD** bonds in **R1** and **R2**; **C** is the adjacent carbon, **D** and **A** are the hydrogen donor and acceptor atoms, respectively.

The evolution of the **DCA** angle of **R1** and **R2** displays a quite similar behavior along $\omega$; it becomes evident that this is a reactive mode to prepare the hydrogen transfer. The **DCA** angle decreases monotonically until the limit of the **TS** region at $\omega_2$, and then it increases sharply to reach the equilibrium value of the product structures. From reactants to $\omega_2$, the **DCA** angle decreases, thus allowing the approach of the donor and acceptor atoms; this process together with the structural rearrangements all over the molecule that takes place in the reactant region might account for an important portion of the activation work that promotes the hydrogen transfer in the forward and reverse reactions. Within the transition state region, the structural rearrangement continues, although with a significantly lower amplitude, as can be confirmed by monitoring the variation of the **DCA** angle by just few degrees in Figure 4.

Figure 4 also shows the evolution along $\omega$ of the **AH** and **DH** bond distances in **R1** and **R2** (lower panel). The **AH** distance decreases monotonically to reach a constant regime at $\omega_2$; **DH** remains constant at the reactant region, but at $\omega_1$ it starts to increase steadily until the products. Because the **DH** distance remains practically constant at the reactant region, the shortening of the **AH** bond is basically due to the decrease in the **DCA** angle. The **DH** and **AH** profiles show clearly that the hydrogenic motion starts at $\omega_1$ and ceases in $\omega_2$. The trends presented in Figure 4 in which the structural reorder is observed all along the reaction coordinate, but with larger amplitude in the reactant and product regions, is recovered when analyzing most structural properties of the systems.

**4.4. Electronic Reordering: Natural Bond Orders.** It has been shown that the hydrogen transfer process is activated by bending and stretching modes of the pyrimidinic backbone; on the other hand, Figure 4 evidenced that the hydrogen transfer is accompanied by structural reordering, especially in the region of the molecule where the donor and acceptor atoms are located. To characterize the change of the electronic density along the reaction coordinate, the **CD** and **CA** natural bond orders have been studied, and their profiles are shown in Figure 5; at the reactant region, the **CD** and **CA** bond orders present slight variations. Note that the difference between the bond order values is smaller in **R1** than in **R2**, thus indicating that electronic delocalization at the reactant region is more favored in **R1** than in **R2**; this is consistent with the observed behavior of the bond distances discussed in the previous paragraphs. Within the **TS**

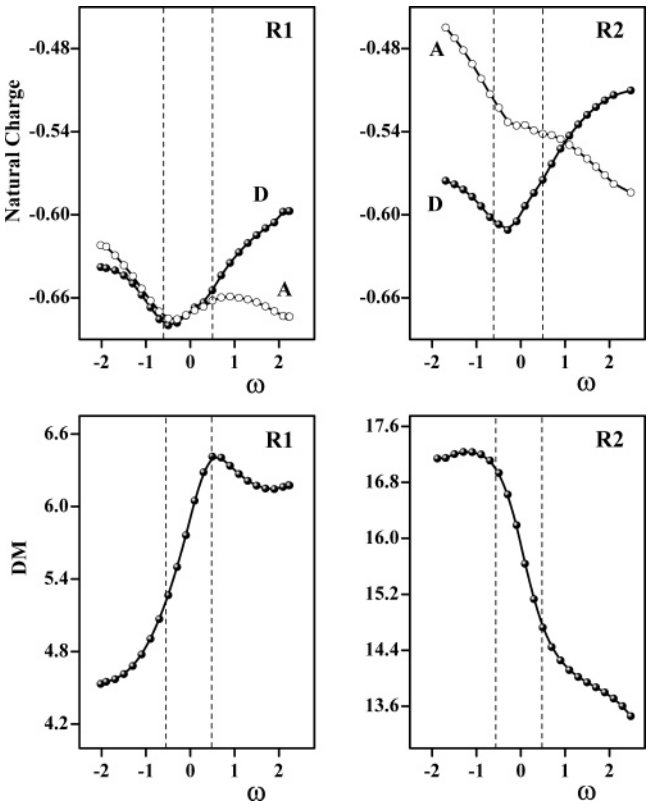


**Figure 6.** Natural charges of hydrogen donor and acceptor atoms and dipole moment (in Debye) profiles for **R1** and **R2** reactions.

region, the bond orders change drastically, indicating a strong electronic reordering with electronic flux in the opposite direction to the hydrogenic motion, the **CD** bond order increases, whereas the **CA** bond order decreases along the reaction coordinate, thus indicating that the electronic and proton transfers follow opposite directions.

The difference between the **CD** and **CA** bond orders indicate that, in **R1**, the reactant region is characterized by a more pronounced delocalization of the electronic charge than the product region. In contrast to this, the electronic delocalization observed now in the product region of **R2** is consistent with the relative low value of the dipole moment displayed in Figure 6. The opposite behavior of the delocalization patterns observed in **R1** and **R2** could explain the difference in their activation work for the forward and reverse reactions, $W_1$ and $W_4$, respectively.

In **R1**, the bond orders profiles cross each other at the transition state where the highest degree of electronic delocalization within the **D**−**C**−**A** backbone is observed. In contrast to this, in **R2**, crossing is achieved at $\omega_2$ when the system initiates its relaxation process. Clearly, the electronic delocalization in the **D**−**C**−**A** atoms is not playing the same role in both reactions: whereas in **R1** delocalization seems to be important in the stabilization of the keto tautomer, in **R2**, it stabilizes the enol form. It is important to stress the fact that the largest variations of the bond orders occur within the transition state region, so it is in this region where most of the electronic reorder takes place.

On the other hand, the crossing points on the bond order profiles in **R1** and **R2** are quite close to the critical points displayed by the profiles of $\mu$ and $\eta$ (see Figure 3). The minimum exhibited by the chemical potential profile ($d\mu/d\omega = 0$) corresponds to a constant charge flux that is consistent with the maximum degree of delocalization shown by the bond order profiles. In this context, the maximum hardness appears to be associated to the highest electronic delocalization within this region of the molecular backbone.

**Natural Charges and Dipole Moments.** Figure 6 displays the profiles of natural charges of the donor and acceptor atoms in **R1** and **R2** (upper panel). The charge separation between the **D** and **A** atoms is very small within the reactant region of **R1**; these split out when entering the product region. In contrast to this, the charge separation in **R2** is quite large all along $\omega$; the charge profiles cross each other when the reaction is well advanced at the product region. These results are confirming that the reactant region in **R1** and the product region in **R2** are characterized by a high electronic delocalization. Our results suggest the charge separation between **D** and **A** induced by Mg(II) in the keto tautomer activates the reaction, and the relaxation process to reach the enol tautomer seems to be driven by the electronic delocalization. Therefore, high values of $W_1$ and $W_4$ for **R1** and **R2**, respectively, are due to strong electronic delocalization that has to be broken to prepare the reaction to continue; this is in agreement with what is observed in the bond order and atomic charge profiles.

It is interesting to notice that the dipole moment profiles of **R1** and **R2** (Figure 6, lower panel) present opposite trends along the reaction coordinate, thus confirming that the presence of the metal cation center induces a different mechanism for the intramolecular hydrogen transfer. The direction of the increase in the electron delocalization is consistent with the direction of the decrease of the dipole moment. It is interesting to stress the fact that DM remains quite constant in the product region of **R1** and in the reactant region of **R2**, thus confirming the opposite behavior of the localization/delocalization patterns in both reactions.

In summary, the analysis of structural and electronic properties along the reaction coordinate indicates that the presence of Mg(II) leads to significative changes in the hydrogen transfer reaction mechanisms. In the direct reaction, the metal cation polarizes the electronic density of the keto tautomer, activating the structural reordering that brings the donor and acceptor atoms as closer as possible to produce the hydrogen transfer that actually occurs within the **TS** region and is accompanied by a strong electronic reordering and by rather weak structural rearrangements.

**4.5. Metal Migration in R2.** After the hydrogen has been transferred and the monocoordinated complex with the enol isomer of thymine has been formed, the migration of the metal begins to take place (Figure 1b). The energy profile describing the Mg migration from enol to the product is displayed in Figure 7a. Note that the migration process of the cation occurs in the molecular plane; a transition state 0.64 kcal/mol higher than the Mg(II)−thymine (enol) monocoordinated tautomer was confirmed. The complete picture we present here for **R2** is in good agreement with a recent experimental and theoretical study, in which the metal cation is found to be bicoordinated by the O4 and N3 atoms.[19] It can be observed that the process is practically free to occur; thus, it can be considered as a spontaneous second step to complete the reaction keto → products. The migration process to reach the bicoordinated complex is exoenergetic by 19 kcal/mol. Figure 7b displays the reaction force profile for the migration process, and it reflects the potential energy of the process, which seems to have an incipient metastable state at about $\omega = 8$. Because the direction of the force is opposite to that of the increasing energy, then as the energy initially increases, the reaction force is negative until the first inflection point of $E(\omega)$ is reached; this is a minimum

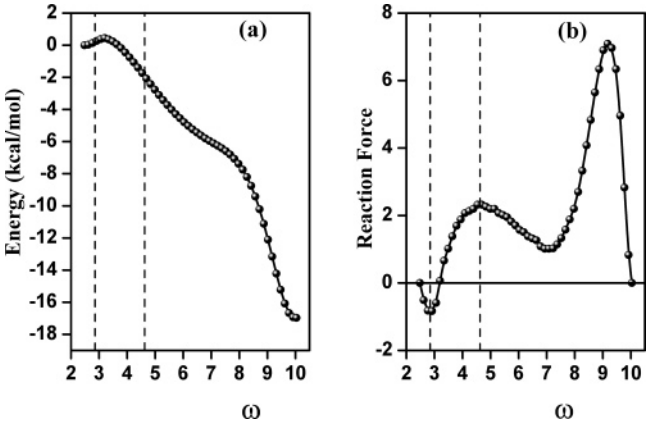


**Figure 7.** (a) Energy (in kcal/mol) and (b) force profiles (in kcal/mol·w) for the migration process of Mg(II) in **R2**.

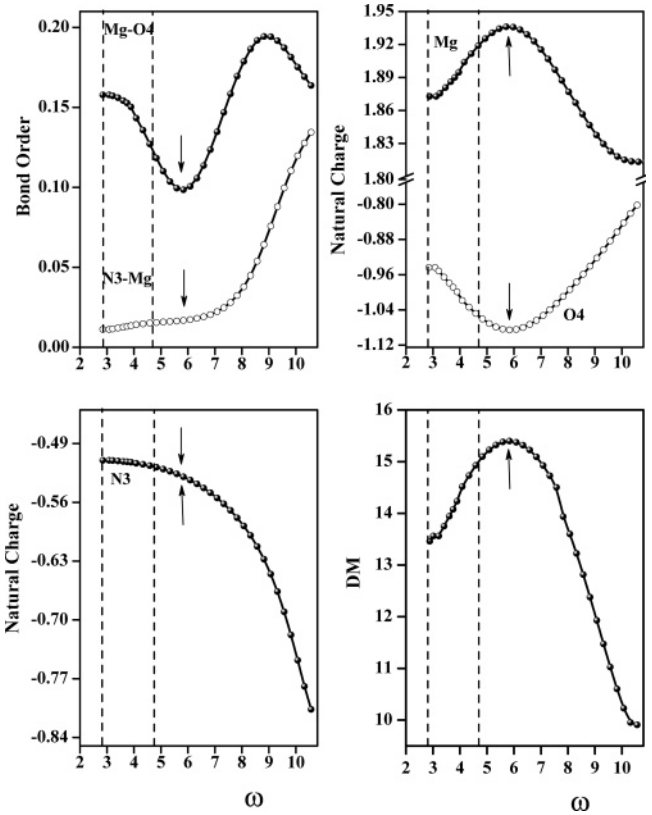


**Figure 8.** Bond orders (Mg−O4 and N3−Mg), natural charges (O4, Mg and N3), and dipole moment (in Debye) profiles for the metal migration process.

in $F(\omega)$. Then the force begins to increase but is still negative, and at the transition state it reaches a value of zero. As the energy starts its decrease, the reaction force is henceforth positive; it reaches critical points (two maxima and a minimum) at the second, third, and fourth inflection points of energy. Because the structural rearrangements other than the Mg migration itself are very small during the process, we analyze few key electronic properties to get more insights on the metal migration process. Figure 8 shows the Mg−O4 and Mg−N3 natural bond order profiles. Although both profiles present small values indicating that the interaction metal−nucleobase is mainly of ionic nature, it is remarkable that these bond orders reach almost the same value when reaching the product, indicating that the electronic charge is highly delocalized at this region of molecular backbone. The minimum of the Mg−O4 bond order is reached when the Mg−O4−C4 angle reaches 180°; this configuration is indicated with an arrow on the curves of Figure 8.

The natural charge profiles of O4 and Mg atoms, also displayed in Figure 8, present opposite behavior along the reaction coordinate; here again, both profiles present a critical point when the Mg−O4−C4 angle equals 180°. At this point, O4 and Mg atoms reach maximum and minimum values of their electronic charge, respectively, thus indicating that here the Mg−thymine interaction is basically ionic; this is in agreement with the Mg−O bond order profile that presents a minimum value at the same point. The natural charge profile for N3 indicates that it remains quite constant until that Mg−O4−C4 angle reach a value of 180°; afterward, it decreases monotonically to reach the value of the final product. The N3 atom gets a considerable amount of electronic charge to allow the ionic coordination with Mg(II). The Mg−N3 bond order and the charge on N3 both seem to begin more rapid changes at about $\omega = 8$, when an incipient metastable state shows up, as already observed in the force profile of Figure 7. The electronic reordering in the Mg−O4−C4−N3 backbone atoms explains the considerable amount of work associated to the metal migration process.

Figure 8 also shows the dipole moment profile for the Mg migration; it also presents a critical point at the configuration where the Mg−O4−C4 angle equals 180°; after this point, it decreases monotonically until reaching the value of the bicoordinated enol complex. This decreasing in DM is expected to be accompanied by an increase in the electron delocalization of the system, which contributes to the high stability of the bicoordinated Mg(II)−thymine(*enol*) complex.

In summary, the metal migration is a free process activated by the hydrogen transfer, and the stabilization of the bicoordinated complex is due to a cooperative effect of the ionic interactions between the metal cation and the nucleobase and an increase in the electronic delocalization on the molecular backbone.

## 5. Conclusions

In this work, energy and force profiles together to the evolution of structural and electronic properties that have been used to characterize the reaction mechanism of the intramolecular proton transfer (keto → enol) in thymine and in its complex with Mg(II). The migration of the metal that takes place in the later system to bring the monocoordinated complex into a bicoordinated one was also analyzed. Our results showed that the presence of a metal cation center lowers the energy barrier of the tautomerization process and result in a considerable stabilization of the enol tautomer. It seems that the charge separation between the donor and acceptor atoms induced by the presence of Mg(II) in the keto tautomer activates the reaction; the relaxation process to reach the enol tautomer appears to be driven by the electronic delocalization. On the other hand, the formation of the Mg(II)−thymine bicoordinated complex, after the migration of the metal, is stabilized by both ionic interactions and the increase of electronic delocalization.

It is worth stressing the usefulness of the interpretative tools used in this paper; the methodology based upon the characterization of the reaction force opens a new perspective to treat chemical reactions and the molecular structures encountered along the reaction coordinate.

**Acknowledgment.** This work has been supported by FONDECYT through Project No 1060590 and by FONDAP Project No 11980002 (CIMAT). E.R. is grateful to DIPUC and

MECESUP (PUC-0004, Red Química UCH-0116) for a graduate fellowship. We thank Dr. Bárbara Herrera for helpful discussions.

## References and Notes

(1) Toro-Labbé, A. *J. Phys. Chem. A* **1999**, *103*, 4398.
(2) Jaque, P.; Toro-Labbé, A. *J. Phys. Chem. A* **2000**, *104*, 995.
(3) Toro-Labbé, A.; Gutiérrez-Oliva, S.; Concha, M. C.; Murray, J. S.; Politzer, P. *J. Chem. Phys.* **2004**, *121*, 4570.
(4) Herrera, B.; Toro-Labbé, A. *J. Chem. Phys.* **2004**, *121*, 7096.
(5) Gutiérrez-Oliva, S.; Herrera, B.; Toro-Labbé, A.; Chermette, H. *J. Phys. Chem. A.* **2005**, *109*, 1748.
(6) Politzer, P.; Toro-Labbé, A.; Gutiérrez-Oliva, S.; Herrera, B.; Jaque, P.; Concha, M. C.; Murray, J. *J. Chem. Sci.* **2005**, *117*, 467.
(7) Politzer, P.; Burda, J. V.; Concha, M. C.; Lane, P.; Murray, J. *J. Phys. Chem. A* **2006**, *110*, 756.
(8) See for example: Gutiérrez-Oliva, S.; Jaque, P.; Toro-Labbé, A. In *Reviews of Modern Quantum Chemistry. A Celebration of The Contributions of Robert G. Parr*; Sen, K. D., Ed.; World Scientific: London, 2002; p 966 and references therein.
(9) Hud, N. V.; Polak, M. *Curr. Opin. Struct. Biol.* **2001**, *11*, 293.
(10) Ferdor, M. J. *Curr. Opin. Struct. Biol.* **2002**, *12*, 289.
(11) Sclavi, B.; Sullivan, M.; Chance, M.; Brenowitz, M.; Woodson, S. *Science* **1998**, *279*, 1940.
(12) Anastassopoulou, J. *J. Mol. Struct.* **2003**, *651*−*653*, 19.
(13) Sponer, J.; Burda, J. V.; Sabat, M.; Leszczynski, J.; Hobza, P. *J. Phys. Chem. A* **1998**, *102*, 5951.
(14) Galaris, D.; Evangelou, A. *Crit. Rev. Oncol. Hematol.* **2002**, *42*, 93.
(15) Anastassopoulou, J.; Theophanides, T. *Crit. Rev. Oncol. Hematol.* **2002**, *42*, 79.
(16) Tajmir-Riahi, H. A.; Theophanides, T. *Inorg. Chim. Acta* **1983**, *80*, 223.
(17) Burda, J. V.; Sponer, J.; Hobza, P. *J. Phys. Chem.* **1996**, *100*, 7250.
(18) Zhu, W.; Luo, X.; Mok Puah, C.; Tan, X.; Shen, J.; Gu, J.; Chen, K.; Jiang, H. *J. Phys. Chem. A* **2004**, *108*, 4008.
(19) Liu, H.; Sun, J.; Hu, Y.; Han, K.; Yang, S. *Chem. Phys. Lett.* **2004**, *389*, 342.
(20) Sun, J.; Liu, H.; Wang, H.; Han, K.; Yang, S. *Chem. Phys. Lett.* **2004**, *392*, 285.
(21) Egli, M.; Gessner, R. V. *Proc. Natl. Acad. Sci.* **1995**, *92*, 180.
(22) Russo, N.; Toscano, M.; Grand, A. *J. Phys. Chem. A* **2003**, *107*, 11533.
(23) Sanz Miguel, P. J.; Lax, P.; Willermann, M.; Lippert, B. *Inorg. Chim. Acta* **2004**, *357*, 4552.
(24) Lippert, B.; Schöllhorn, U.; Thewalt, H. *J. Am. Chem. Soc.* **1986**, *108*, 6616.
(25) Osama, K.; Abou-Zied, R. J.; Floyd, E. R. *J. Am. Chem. Soc.* **2001**, *123*, 4613.
(26) Watson, J. D.; Crick, F. H. C. *Cold Spring Harbor Symp. Quantum Biol.* **1953**, *18*, 123.
(27) Podolyn, Y.; Gorb, L.; Leszczynski, J. *Int. J. Mol. Sci.* **2003**, *4*, 410.
(28) Danilov, V. I.; Anisimov, V. M.; Kurita, N.; Hovorun, D. *Chem. Phys. Lett.* **2005**, *412*, 285.
(29) Marcus, R. A. *Annu. Rev. Phys. Chem.* **1964**, *15*, 155.
(30) Martínez, J.; Toro-Labbé, A. *Chem. Phys. Lett.* **2004**, *392*, 132.
(31) Hammond, G. S. *J. Am. Chem. Soc.* **1955**, *77*, 334.
(32) Bulat, F. A.; Toro-Labbé, A. *J. Phys. Chem. A* **2003**, *107*, 3987.
(33) Leffler, J. E. *Science* **1953**, *117*, 340.
(34) Solà, M.; Toro-Labbé, A. *J. Phys. Chem. A* **1999**, *103*, 8847.
(35) Parr, R. G.; Yang, W. *Density Functional Theory of Atoms and Molecules*; Oxford University Press: New York, 1989.
(36) Geerlings, P.; De Proft, F.; Langenaeker, W. *Chem. Rev.* **2003**, *103*, 1793.
(37) Parr, R. G.; Donnelly, R. A.; Levy, M.; Palke, W. E. *J. Chem. Phys.* **1978**, *68*, 3801.
(38) Parr, R. G.; Pearson, R. G. *J. Am. Chem. Soc.* **1983**, *105*, 7512.
(39) Parr, R. G.; Zhou, Z. *Acc. Chem. Res.* **1993**, *26*, 252.
(40) Becke, A. D. *J. Chem. Phys.* **1993**, *98*, 5648.
(41) Møller, C.; M. Plesset, S. *Phys. Rev.* **1934**, *46*, 618.
(42) Peng, C.; Ayala, P. Y.; Schlegel, H. B.; Frisch, M. J. *J. Comput. Chem.* **1996**, *17*, 49.
(43) Fukui, K. *Acc. Chem. Res.* **1981**, *14*, 363.
(44) Reed, A. E.; Curtiss, L. A.; Weinhold, F. *Chem. Rev.* **1988**, *88*, 899.
(45) Frisch, M. J.; Trucks, G. W.; Schlegel, H. B.; Scuseria, G. E.; Robb, M. A.; Cheeseman, J. R.; Montgomery, J. A., Jr.; Vreven, T.; Kudin, K. N.; Burant, J. C.; Millam, J. M.; Iyengar, S. S.; Tomasi, J.; Barone, V.; Mennucci, B.; Cossi, M.; Scalmani, G.; Rega, N.; Petersson, G. A.; Nakatsuji, H.; Hada, M.; Ehara, M.; Toyota, K.; Fukuda, R.; Hasegawa, J.; Ishida, M.; Nakajima, T.; Honda, Y.; Kitao, O.; Nakai, H.; Klene, M.; Li, X.; Knox, J. E.; Hratchian, H. P.; Cross, J. B.; Bakken, V.; Adamo, C.; Jaramillo, J.; Gomperts, R.; Stratmann, R. E.; Yazyev, O.; Austin, A. J.; Cammi, R.; Pomelli, C.; Ochterski, J. W.; Ayala, P. Y.; Morokuma, K.; Voth, G. A.; Salvador, P.; Dannenberg, J. J.; Zakrzewski, V. G.; Dapprich, S.; Daniels, A. D.; Strain, M. C.; Farkas, O.; Malick, D. K.; Rabuck, A. D.; Raghavachari, K.; Foresman, J. B.; Ortiz, J. V.; Cui, Q.; Baboul, A. G.; Clifford, S.; Cioslowski, J.; Stefanov, B. B.; Liu, G.; Liashenko, A.; Piskorz, P.; Komaromi, I.; Martin, R. L.; Fox, D. J.; Keith, T.; Al-Laham, M. A.; Peng, C. Y.; Nanayakkara, A.; Challacombe, M.; Gill, P. M. W.; Johnson, B.; Chen, W.; Wong, M. W.; Gonzalez, C.; Pople, J. A. *Gaussian 03*, revision C.02; Gaussian Inc.: Wallingford, CT, 2004.
(46) Linstrom, P. J., Mallard, W. G., Eds. *NIST Chemistry WebBook, NIST Standard Reference Database Number 69*; National Institute of Standards and Technology, (http://webbook.nist.gov), Gaithersburg MD, 20899, June 2005.
(47) Kistenmacher, T. J.; Eichhorn, G. L. *Nucleic Acids-Metal Ion Interactions*; Spiro, T. G., Ed.; Wiley: New York, 1980.
(48) Camerman, N.; Fawcett, J. K. *J. Mol. Biol.* **1976**, *107*, 601.